ORIGINAL PAPER

Sanguinarine inhibits the proliferation of BGC-823 gastric cancer cells via regulating miR-96-5p/miR-29c-3p and the MAPK/JNK signaling pathway

Xian-Zhe Dong[1] · Yan Song[1] · Yu-Pan Lu[2] · Yuan Hu[3] · Ping Liu[3] · Lan Zhang[1]

Abstract

Sanguinarine (SAN), a quaternary benzophenanthridine alkaloid extracted from the root of Papaveraceae plants, has shown antitumour effects in multiple cancer cells. However, the therapeutic effects and the underlying mechanisms of SAN in gastric cancer (GC) remain elusive. In this study, the in vitro proliferation inhibition effect of SAN in GC cells was determined using CCK-8 assay, the in vivo antitumor effect of SAN was evaluated in mice with xenotransplanted tumor. The mechanism underlying the antitumor activity of SAN was explored by gene microarray assay and bioinformatics analysis. The levels of differentially expressed miRNAs and target genes were verified by real-time RT-PCR and immunohistochemistry. SAN inhibited the proliferation of BGC-823 cells in a concentration-dependent manner in vitro and in vivo. The miR-96-5p and miR-29c-3p were significantly upregulated in untreated BGC-823 cells and significantly downregulated in SAN treated cells. The mRNA and protein expression of their target gene MAP4K4 were upregulated in SAN treated xenotransplanted tumors, and pMEK4 and pJNK1 proteins in the MAPK/JNK signaling pathway were also upregulated by SAN. These indicate that SAN may inhibit the proliferation of BGC-823 cells through the inhibition of miR-96-5p and miR-29c-3p expression, and subsequent activation of the MAPK/JNK signaling pathway.

Keywords Sanguinarine · Gastric cancer · MicroRNAs · Target mRNAs · MAPK/JNK signaling pathway

Introduction

Gastric cancer (GC) is the fourth common malignancy and the second leading cause of cancer death worldwide, although the incidence and mortality of GC have significantly declined in recent decades [1]. Over 70% of GC and GC-related deaths occur in developing countries [2], and almost 50% of the patients are Chinese [3]. Unfortunately, the symptoms of GC are non-specific at the early stage [4], and more than 80% of the patients were diagnosed at advanced stages [5]. Currently, combination chemotherapeutic regimens (two or three-cytotoxic drug regimens) are available for the treatment of advanced GC [6]. However, the objective response rate is unsatisfactory. Therefore, developing more effective chemotherapeutic agents for GC is urgently needed.

Sanguinarine (SAN) [13-methyl(1,3) benzodioxolo(5,6-c)-1,3-dioxolo(4,5) phenanthridinium] is a benzophenanthridine alkaloid (Fig. 1) that is extracted from the root of *Sanguinaria canadensis* and other poppy-fumaria species [7]. It has been used in many over-the-counter products such as toothpaste and mouthwash [8] due to its broad-spectrum pharmacological properties such as antimicrobial, anti-inflammatory, and antioxidative activities [9]. Studies have indicated that SAN possesses cytotoxic and cytostatic effects in a variety of human cancer cells, including lung adenocarcinoma cells, bladder cancer cells, prostate cancer cells,

✉ Ping Liu
  cpi301@163.com

✉ Lan Zhang
  lanizhg@126.com

  Xian-Zhe Dong
  dongxianzhe@163.com

[1] Department of Pharmacy, Xuanwu Hospital of Capital Medical University, 45 Changchun Road, Xicheng District, 100053 Beijing, China

[2] Department of Pharmacy, Chinese PLA General Hospital, 100853 Beijing, China

[3] Department of Clinical Pharmacology, Pharmacy Care Center, Chinese PLA General Hospital, 28 Fuxing Road, Haidian District, 100853 Beijing, China
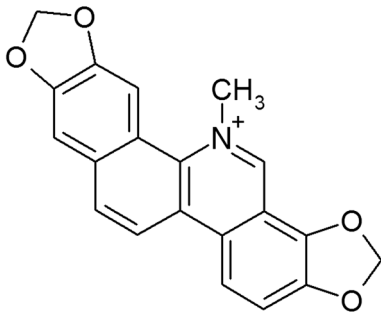
Fig. 1 Chemical structure of SAN

colorectal cancer cells, melanoma, and pancreatic cancer cells [10–14]. Notably, the antiproliferative and apoptotic induction activity of SAN is cancer cell-specific and SAN is harmless to normal cells. A study found that SAN exhibited antiproliferative effect in human epidermoid carcinoma cells (A431), but not in normal human epidermal cells [15]. Similarly, mouse lymphocytic leukemic cells are more sensitive to SAN than normal spleen cells [16]. Therefore, as a potential chemotherapeutic agent, SAN has gained more and more attention. However, little is known about the effects of SAN in GC, and the precise mechanism of SAN-induced anticancer effect has not been completely elucidated [17]. We found that SAN inhibits the proliferation of BGC-823 human GC cells through regulating the expression of miR-96-5p and miR-29c-3p and the MAPK/JNK signaling pathway. Our findings may facilitate the discovery of diagnostic markers and therapeutic targets for gastric cancer and provide useful information for the development of new therapeutic agents.

Materials and methods

Cell culture

Human gastric cancer MGC-803, BGC-823 and SGC-7091 cell lines and the human gastric mucosa epithelial GES-1 cell line were purchased from Cancer Hospital Chinese Academy of Medical Sciences (Beijing, China). MGC-803, BGC-823 and SGC-7901 cells were cultured in RPMI-1640 medium (HyClone, USA) supplemented with 10% heat-inactivated fetal bovine serum (FBS; HyClone, USA), and GES-1 cells were cultured in DMEM medium (HyClone, USA) supplemented with 10% heat-inactivated FBS in a humidified cell incubator with 5% CO_2 at 37 °C.

In vitro cell viability assay

MCF-7, LS-180, Hela, HepG2, BGC-823, MGC-803 and SGC-7901 cells were seeded in 96-well plates at 3000 cells/well in 90 μL 10% RPMI-1640. The cells were cultured

overnight and treated with SAN (National Institutes for Food and Drug Control, China) at six concentrations: 0, 50, 100, 200, 300, and 400 μmol/L for 24/48 h and the corresponding blank control of reagents was also set. Each concentration was repeated in four wells. Cell viability was assessed using the Cell Counting Kit-8 (CCK-8; Biosharp, Beijing, China) according to the manufacturer's protocol. After the cells were incubated with CCK-8 for 4 h, the optical density of the cells was measured using an 1420-012 Multilabel Counter (PerkinElmer, USA) at a wave length of 450 nm. All reactions were run in triplicate. The inhibition rate was calculated by the optical density value, and the anti-proliferative effect of SAN was expressed as IC_{50} value. All data are presented as mean ± SE.

Tumor xenograft

BGC-823 cell line was used to establish a subcutaneous xenotransplanted tumor model in BALB/c-nude mice [Beijing Vital River Laboratories, Beijing, China; License No: SCXK (Jing) 2016-0006]. The animals were maintained under a 12/12 h light–dark cycle in a temperature and humidity-conditioned environment, and had free access to food and water. Then 1.5×10^6 BGC-823 cells were suspended in 0.2 mL serum free RPMI-1640 medium, and implanted subcutaneously into the foreleg of nude mice. One week after implantation, the mice were randomly divided into five groups: model group, positive control group [5-fluorouracil (5-FU) (Xudonghai Pharmaceutica CO, Shanghai, China) 50 mg/kg], SAN low dose group (2.5 mg/kg), SAN medium dose group (5 mg/kg) and SAN high dose group (10 mg/kg). SAN was administered intraperitoneally every other day. The tumor length and width were measured once every other day, the volume of tumor was calculated by the formula $(L \times W^2)/2$ (L: tumor length, W: tumor width). The tumor weight was measured at sacrifice and recorded. HE staining was performed to determine the changes of pathological morphology of transplanted tumor tissue.

Gene microarray assay

To reveal miRNA profiling in response to SAN treatment in BGC-823 cells, we examined the expression of miRNAs in BGC-823 cells after SAN treatment using microarrays. GES-1 and BGC-823 cells were seeded at a density of 2×10^6 cells/well in 6-well plates and cultured at 37 °C in a humid environment containing 5% CO_2 overnight. One well of BGC-823 cells was treated with SAN at a concentration of 250 μmol/L for 24 h. After 24 h of treatment, total RNAs of GES-1, untreated and treated BGC-823 cells were extracted using Trizol reagent (Invitrogen, USA) according to the manufacturer's instructions. The quality of the total RNA was assessed by SAM3000 spectrophotometry (Meriton,

Beijing, China) and electrophoresis on 1.5% agarose formaldehyde denaturing gels (Biorad, USA). The samples were labeled using the FlashTag® Biotin HSR RNA Labeling Kit and WT Terminal Labeling Kit (Affymetrix, USA) and hybridized to the miRNA and mRNA chip in a Hybridization Oven 640 (Affymetrix, USA). The arrays were scanned with Affymetrix GeneChip Scanner 3000 7G (Affymetrix, USA) to generate the data.

Bioinformatics studies

Differential expression analyses (GES-1 vs untreated BGC-823, untreated BGC-823 vs SAN treated BGC-823) were performed, P value < 0.05 and Fold change ≥ 1.2 were chosen as the thresholds to screen the differentially expressed miRNAs. Gene intersections in the three types of cells were obtained. The target genes of differentially expressed miRNAs were predicted using miRanda algorithms, and screened for fold change ≥ 2.5 or ≤ -2.5. Significant pathways were selected by Pathway-analysis. Differentially expressed genes were used for Kyoto Encyclopedia of Genes and Genomes (KEGG) pathway analyses between groups. Fisher exact test was used in Pathway analyses. Benjamini–Hochberg step-up method was applied to calculate the P value of each pathway,

which was then rectified using false discovery rate (FDR) method. $P < 0.05$ was considered statistically significant. Besides, the enrichment level of each pathway was assessed by enrichment score.

## Validation of differentially expressed gene by RT-PCR

RT-PCR was performed to validate the expression level of selected differentially expressed genes identified by microarray. Gene-specific primers are listed in Table 1 (AUGCT, Beijing, China). Total RNA for RT-PCR was extracted from GES-1, untreated and 250 μmol/L SAN treated BGC-823, MGC-803 and SGC-7901 cells using Trizol reagent and reverse transcribed to cDNA using miRcute Plus miRNA First-Strand cDNA Synthesis Kit (TIAN GEN, Beijing, China) at 42 °C for 60 min and 95 °C for 3 min. Real-time quantitative PCR was performed in 25 μL reaction solution containing 2 μL the first strand cDNA, 1 μL forward and 0.5 μL reverse primers at 200 nM, 12.5 μL 2 × miRcute Plus miRNA Premix and 9 μL ddH$_2$O. The PCR process consisted of template denaturation, miRNAs enrichment and 45 cycles of 20 s denaturation at 94 °C and 34 s annealing at 60 °C. All reactions were run in triplicate. Reaction and

Table 1 The primer sequences of miRNAs and mRNAs

| Name	Sequence	Long
U6-F	5′-AATCTAGCTGCTGCGGTTCC-3′	20
has-miR-454-3p-F	5′-TCTGTTTATCACCAGATCCT-3′	20
has-miR-18b-5p-F	5′-TAAGGTGCATCTAGTGCAGTTAG-3′	23
has-miR-148b-3p-F	5′-TCAGTGCATCACAGAACTTTG-3′	21
has-miR-330-5p-F	5′-TCTCTGGGCCTGTGTCTTAGG-3′	21
has-miR-26b-5p-F	5′-TTCAAGTAATTCAGGATAGGT-3′	21
miR-29c-3p-F	5′-ACACTCCAGCTGGGTAGCACCATTTGAAAT-3′	30
miR-96-5p-F	5′-TTTGCTTGTGTCTCTCCGCT-3′	20
miR-194-3p-F	5′-CCTGTAACAGCAACTCCATG-3′	20
GAPDH-175F	5′-GTGGAGTCCACTGGCGTCTT-3′	20
GAPDH-175R	5′-GTGCAGGAGGCATTGCTGAT-3′	20
CPS1-F	5′-GCCAAGGGGCCATTGAAAAG-3′	20
CPS1-R	5′-ACCTTGGTGGCCACATCAAT-3′	20
MAP4K4-F	5′-GAGGAAGGCCAGAGGTTGAAA-3′	21
MAP4K4-R	5′-TGGATCATAGAGTGTGGGTTCT-3′	22
PDE1A-F	5′-GCTGGAAAGAATCAGGAGTAGC-3′	22
PDE1A-R	5′-GCTTAACATTGTGGAGCCCAG-3′	21
PDE8B-F	5′-CACGAGGCACTACACCAAGT-3′	20
PDE8B-R	5′-GCACAACATACTGCATGGGC-3′	20
TLL-F	5′-GTATCAGAACGGGGCTCTCG-3′	20
TLL-R	5′-AAATCTCTTCTGGTGGCCCG-3′	20
FRZB-F	5′-TCATCAAGTACCGCCACTCG-3′	20
FRZB-R	5′-ATCAGCTCCGTCCGCAGTAA-3′	20
PTGS2-F	5′-CTGCCCTTCTGGTAGAAAAGC-3′	21
PTGS2-R	5′-GCTTCCAGTAGGCAGGAGAAC-3′	21

(A)

(B)

(C)

(D)

(E)

(F)
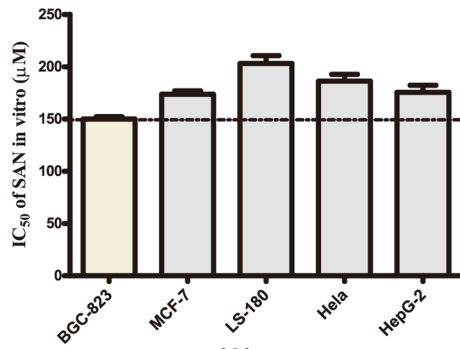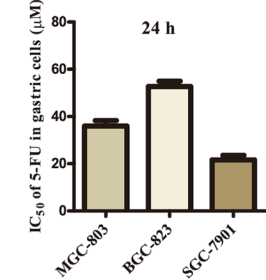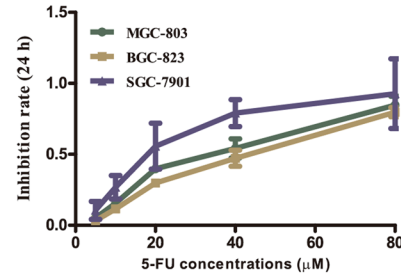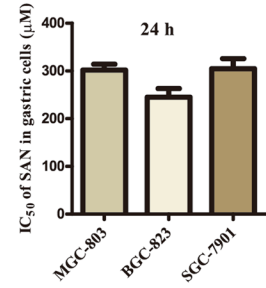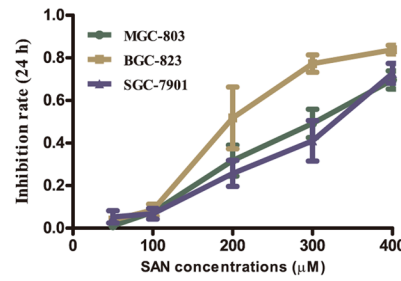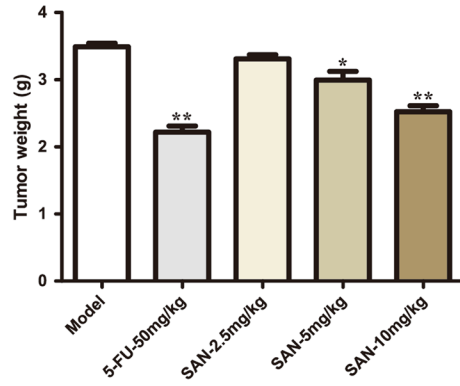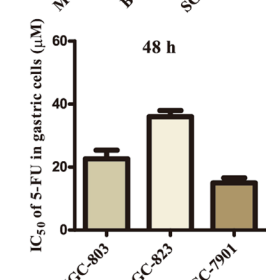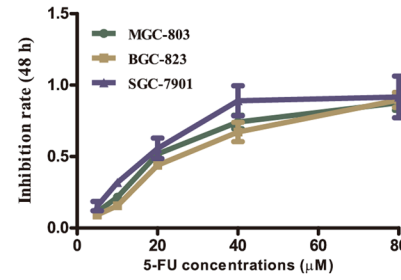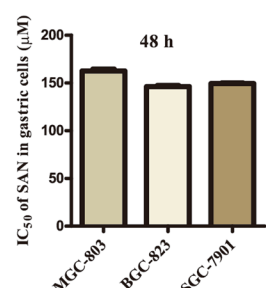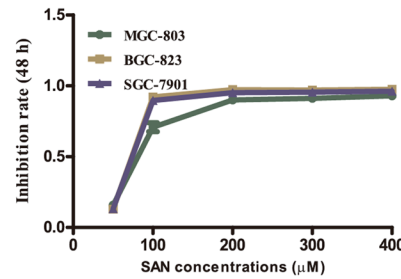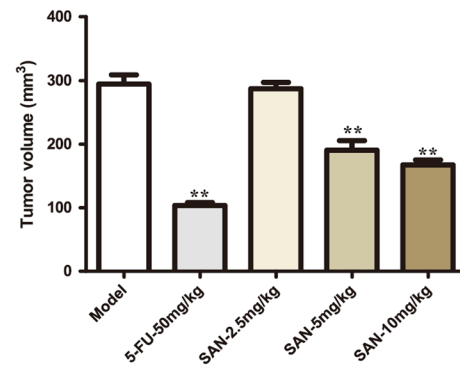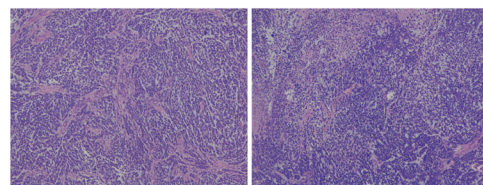
Model   5-FU-50mg/kg
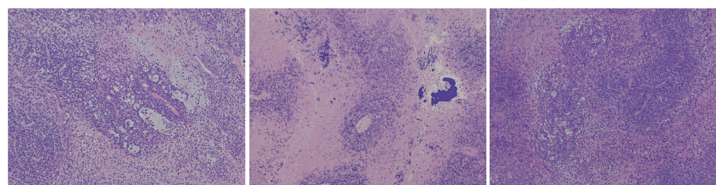
SAN-2.5mg/kg   SAN-5mg/kg   SAN-10mg/kg

◄Fig. 2 SAN inhibited the proliferation of GC cells in vitro and in vivo. **a** Proliferation inhibition effect of SAN in five tumor cell lines after 48 h treatment evaluated by CCK-8 assay. **b**, **c** Inhibition rates and IC_{50} values of SAN in three GC cell lines evaluated by CCK-8 assay. MGC-803, BGC-823, and SGC-7901 cells were incubated with 0, 50, 100, 200, 300, 400 μmol/L SAN for 24 h (**b**) or 48 h (**c**). The proliferation inhibition rate and IC_{50} values were determined at the end of the treatments. **d**, **e** Effect of SAN on the growth of BGC-823 xenograft tumor in nude mice. One week after the implantation of BGC-823 cells, the mice were randomly divided into five groups: three groups received different doses of SAN, one group received 5-FU as the positive control, and a model group as the negative control. The effect of SAN on tumor weight (**d**) and tumor volume (**e**) were detected, $n = 10$. **f** HE staining of xenograft tumor tissues. HE staining was performed to identify the effect of SAN on the pathomorphology of GC cells. Original magnification: ×100. Each data represented the mean ± SD from three independent experiments. *$P < 0.05$, **$P < 0.01$, compared with the model group

signal detection were measured using RT-PCR Detection system (Bio-Rad, USA). The cDNA synthesis and PCR of mRNAs were performed using iScriptTM cDNA Synthesis and SsoFastTM EvaGreen Supermix Kits (Bio-Rad, USA). The reaction procedure was set according to the manufacturer's instructions. The CT values of miRNAs and mRNAs were converted into absolute copy numbers using standard curves of GAPDH and U6 miRNA.

Determination of protein expression by immunohistochemistry

The expression levels of MAP4K4, pJNK1, and pMEK4 proteins in paraffin-embedded xenotransplanted GC tumor tissue slices were examined by immunohistochemistry. The tissue slices were incubated in 3% hydrogen peroxide solution at room temperature in dark for 25 min to inhibit the activity of endogenous hyperoxidase. The slices were washed three times with PBS for 5 min. After the inactivation of hyperoxidase, the slices were incubated in 3% BSA for 30 min at room temperature, and further incubated with the primary antibodies of MAP4K4 (Abcam (ab155583)), pMEK4-(phospho S80, Abcam (ab39403)), and pJNK1-(phospho T183+Y185, Abcam (ab46821)) at certain dilution (MAP4K4, 1:1000; pMEK4, 1:500; pJNK1, 1:500) overnight at 4 °C. Afterword, the samples were washed with PBS for three times, with 5 min each time. The secondary antibody, goat anti-rabbit horseradish peroxidase (HRP) (KPL), was added to the tissue slices dropwise and incubated for 50 min at room temperature. After the slices were washed three times with PBS, a few drops of freshly prepared DAB solution was added to the slices for color reaction. Subsequently, the slices were washed with PBS to stop coloring. The nuclei of the cells were stained with haematin for 3 min. After a standard dehydration procedure, the samples were observed under the microscope.

Statistical analysis

All statistic analysis was accomplished using SPSS 17.0 and GraphPad prism 5.0 software (GraphPad Software Inc, San Diego, CA). All independent experiments were performed in triplicate. The data are expressed as mean ± SE, and were analyzed by t test. P value < 0.05 was considered statistically significant.

Results

SAN reduced the viability of GC cells in vitro and in vivo

We first evaluated the effect of SAN on the viability of five different tumor cell lines. For 48 h treatment, BGC-823 was the most sensitive to SAN among the five cancer cell lines (Fig. 2a). Then the proliferation inhibition activities of SAN and 5-FU were determined in three GC cell lines (MGC-803, BGC-823 and SGC-7901). A significant dose-dependent proliferation inhibition effect of SAN was observed in all three GC cell lines after 24 h/48 h treatment (Fig. 2b, c).

To determine whether SAN inhibits tumor growth in vivo as it did in vitro, we subcutaneously implanted SAN sensitive BGC-823 cells into nude mice. We found that 4 weeks administration of SAN reduced the tumor volume and weight in a dose-dependent manner (Fig. 2d, e). HE staining showed that the tumor tissue samples of the five groups contained different degrees of necrosis. SAN-induced necrosis was dose-dependent and was larger in treated groups than in the model group. In the 10 mg/kg SAN treated group, the necrosis area showed obvious calcification (Fig. 2f).These results demonstrated that SAN had antitumor activity in BGC-823 cells in vivo.

Differentially expressed miRNAs and mRNAs in GC cells treated with SAN

SAN exhibited proliferation inhibition effect in BGC-823 cells in vitro and in vivo. Thus, we further investigated the underlying molecular mechanism of the anti-tumor activity of SAN by gene microarray analysis. The absorbance ratios OD_{260}/OD_{280} of the total RNAs extracted from GES-1, untreated BGC-823 cells and SAN (250 μmol/L) treated BGC-823 cells were between 1.8 and 2.1. We found that eight miRNAs and seven mRNAs were differentially expressed in BGC-823 cells following SAN treatment (Fig. 3a, b). Levels of eight miRNAs including miR-194-3p, miR-148b-3p, miR-96-5p, miR-330-5p, miR-454-3p, miR-29c-3p, miR-18b-5p and miR-26b-5p (Fig. 3c–j), and seven mRNAs including CPS1, MAP4K4, PDE1A, PTGS2, PDE8B, TLL, and FRZB (Fig. 4a–g) were verified by PCR.
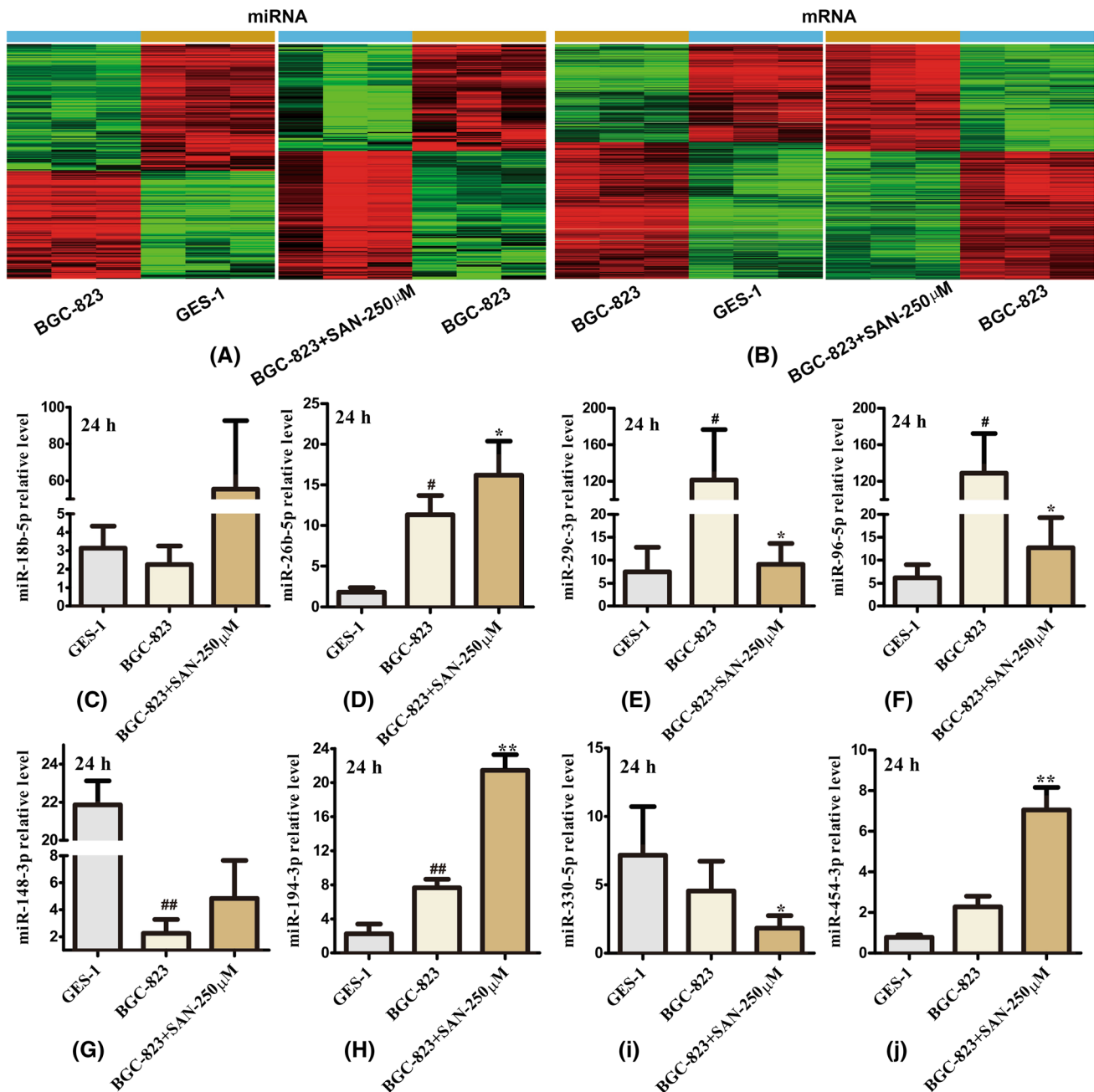
Fig. 3 Analysis of differentially expressed miRNAs in GES-1, untreated and SAN treated BGC-823 cells. **a** Cluster analysis of differentially expressed miRNAs between GES-1 and untreated BGC-823 cells and between untreated and SAN treated BGC-823 cells by microarray assay. **b** Cluster analysis of differentially expressed mRNAs between GES-1 and untreated BGC-823 cells and between untreated and SAN treated BGC-823 cells by microarray assay. Each column represents a sample and each row represents the expression level of a gene. Green color represents low expression and red color represents high expression. There was **c–j** RT-PCR analysis of the expression of eight differentially expressed miRNAs. The relative expression levels of miR-18b-5p (**c**), miR-26b-5p (**d**), miR-29c-3p (**e**), miR-96-5p (**f**), miR-148-3p (**g**), miR-194-3p (**h**), miR-330-5p (**i**), and miR-454-3p (**j**) in GES-1, untreated and SAN treated BGC-823 cells were determined by RT-PCR. [#]$P < 0.05$, [##]$P < 0.01$, compared with GES-1; [*]$P < 0.05$, [**]$P < 0.01$, compared with untreated BGC-823

Compared with that in untreated GES-1 cells, the expression of miR-96-5p and miR-29c-3p was significantly upregulated in untreated BGC-823 cells and significantly downregulated in SAN treated cells, which indicated that miR-96-5p and miR-29c-3p were closely related to the proliferation of BGC-823 cells and was involved in the anti-tumor effect of SAN.

The expression of MAP4K4, CPS1 and PDE1A were consistent with the microarray results. Compared with that in
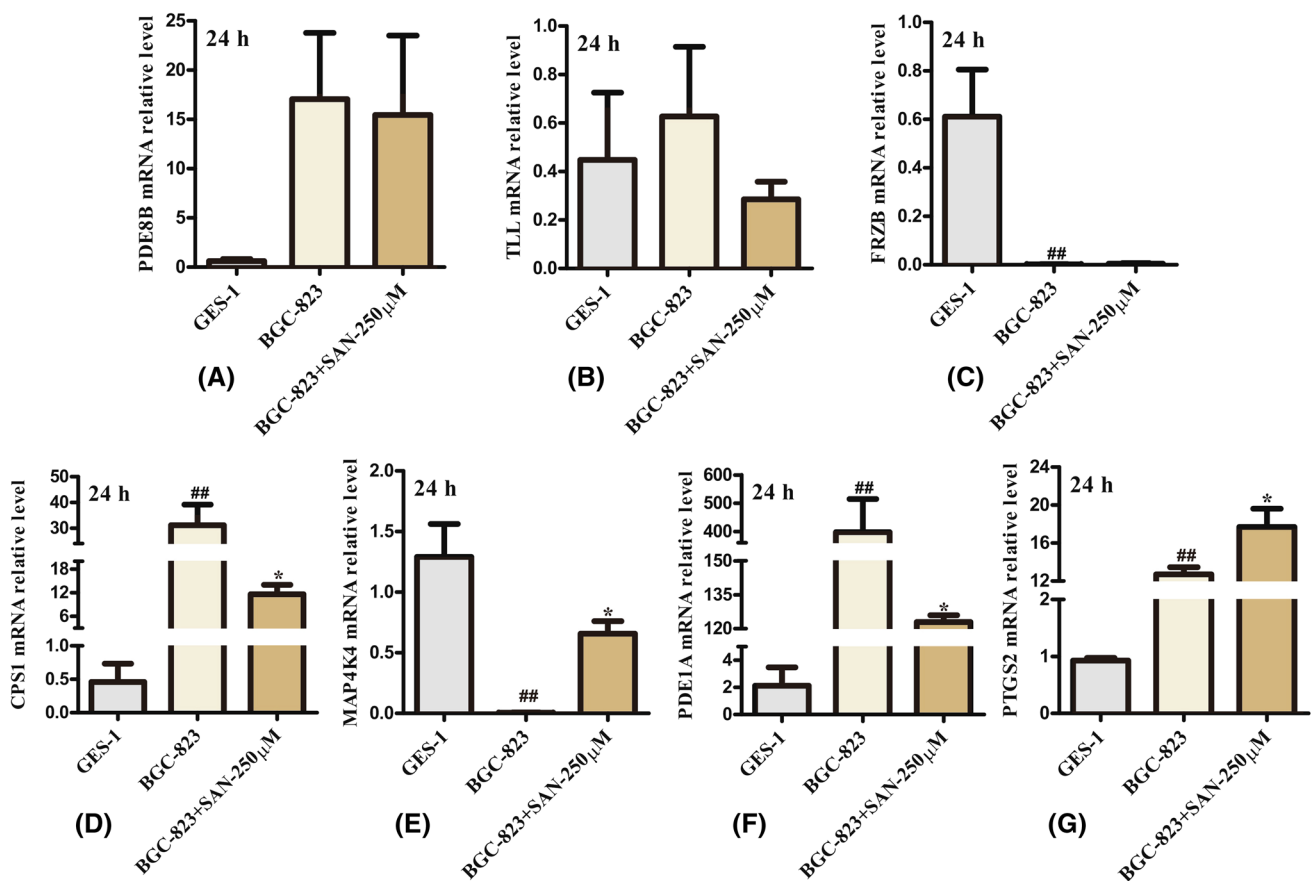
Fig. 4 RT-PCR analysis of the expression of seven differentially expressed mRNAs. The relative expression levels of PDE8B (**a**), TLL (**b**), FRZB (**c**), CPS1 (**d**), MAP4K4 (**e**), PDE1A (**f**), and PTGS2 (**g**) in GES-1, untreated and SAN treated BGC-823 cells were determined by RT-PCR. $^{\#\#}P < 0.01$, compared with GES-1; $^{*}P < 0.05$, compared with untreated BGC-823

GES-1 cells, the expression of CPS1 and PDE1A mRNAs were significantly upregulated in untreated BGC-823 cells and significantly downregulated in SAN treated BGC-823 cells; the expression of MAP4K4 mRNA was significantly downregulated in untreated BGC-823 cells and significantly upregulated in SAN treated BGC-823 cells. These findings indicated that MAP4K4, CPS1 and PDE1A mRNAs were closely related to the anti-tumor effect of SAN. Effects of SAN on the levels of miR-96-5p, miR-29c-3p and MAP4K4 mRNA in MGC-803 and SGC-7901 cells showed the same trend (Fig. 5).

Possible target genes and enriched pathways of miR-29c-3p and miR-96-5p

To explore possible target genes and signaling pathways involved in the response of BGC-823 cells to SAN, we used miRanda to predict the targets of miR-96-5p and miR-29c-3p, which were up-regulated in untreated BGC-823 cells and down-regulated by SAN, compared with their expression in GES-1 cells. The results showed that miR-96-5p and miR-29c-3p had 1805 possible targets. We further analyzed the enriched KEGG pathways for these 1805 targets and found 149 pathways. Among these targets and pathways, six targets (Fig. 6a) and eight pathways (Fig. 6c) were related to cancer, including the mitogen-activated protein kinase (MAPK) signaling pathway and the calcium signaling pathway.

We performed bioinformatic analysis using TargetScan and miRanda software to identify the target genes for miR-96-5p and miR-29c-3p, and found that MAP4K4 and TLL1 were two potential common target genes of these two miRNAs (Fig. 6a). The potential binding sites of miR-96-5p and miR-29c-3p on MAP4K4 and TLL1 mRNAs were also predicted (Fig. 6b). Previous analysis of MAP4K4 showed that the expression of MAP4K4 was negatively correlated with the expression of miR-96-5p and miR-29c-3p, suggesting that MAP4K4 was the target gene of miR-96-5p and miR-29c-3p.
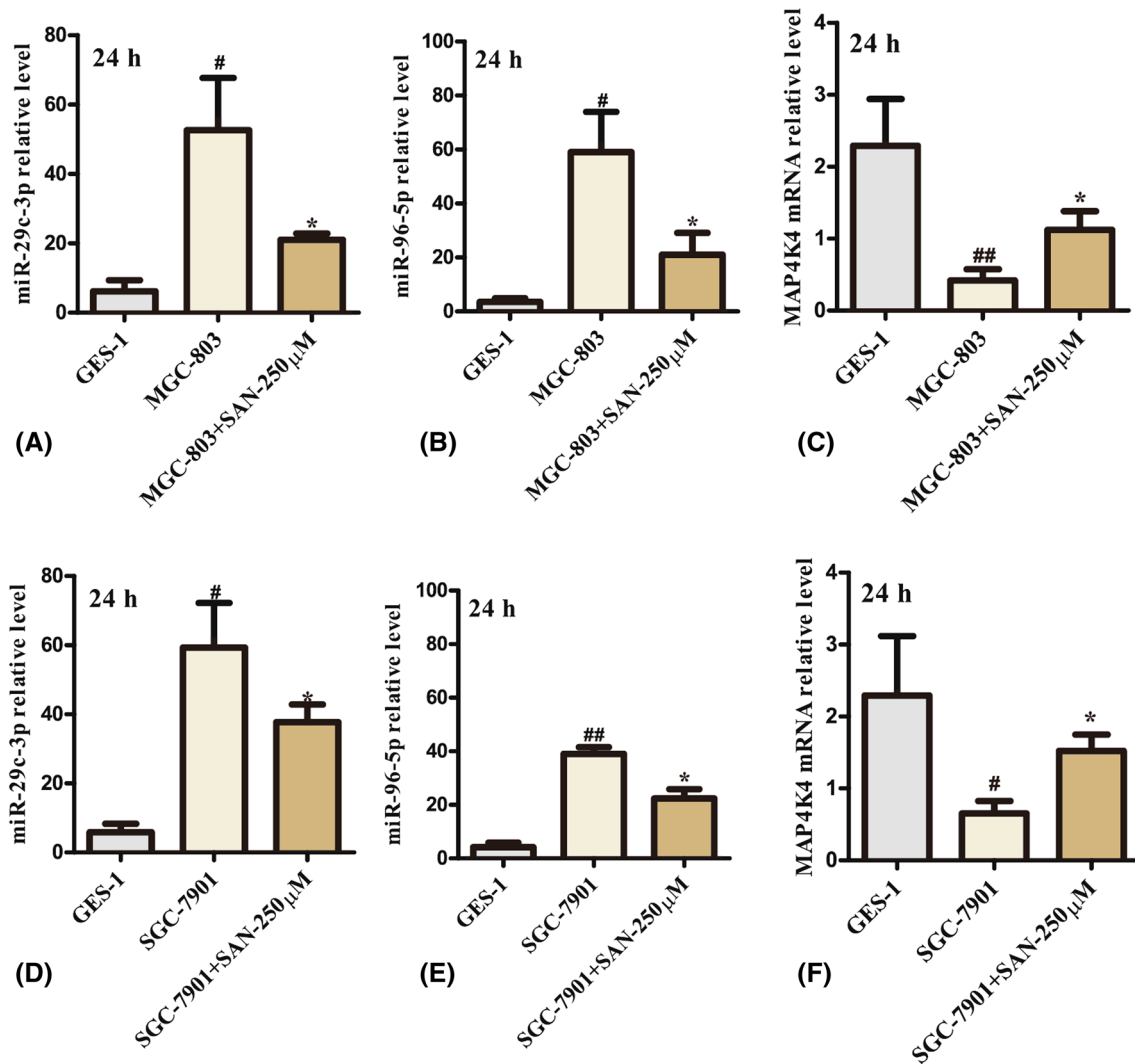
Fig. 5 RT-PCR analysis of the expression of miR-29c-3p, miR-96-5p and MAP4K4 mRNA in MGC-803 and SGC-7901 cells. The relative expression levels of miR-29c-3p (**a**), miR-96-5p (**b**), and MAP4K4 mRNA (**c**) in MGC-803 cells and miR-29c-3p (**d**), miR-96-5p (**e**) and MAP4K4 mRNA (**f**) in SGC-7901 cells were determined by RT-PCR. #$P < 0.05$, ##$P < 0.01$, compared with GES-1; *$P < 0.05$, compared with untreated MGC-803 or untreated SGC-7901 cells

SAN increased the expression of MAP4K4, pMEK4 and pJNK1 proteins

The impact of SAN on the protein expression of MAP4K4, pMEK4 and pJNK1 in gastric tumors were detected by immunohistochemistry analysis. We found that SAN treatment up-regulated the three proteins in a dose-dependent manner (Fig. 7a–f). The expression of MAP4K4, pMEK4 and pJNK1 in SAN treated tumors were in a similar pattern. Compared with those in the model group, the levels of MAP4K4, pMEK4 and pJNK1 were unchanged in SAN low dose (2.5 mg/kg) group, but were markedly up-regulated in SAN medium dose (5 mg/kg) group and high dose (10 mg/kg) group ($P < 0.05$).

Discussion

Gastric cancer is one of the most common malignancies worldwide, with poor prognosis and high mortality rate [18]. Although much effort has been made to improve the diagnosis and treatment of GC, the treatment outcome of gastric cancer is unsatisfactory [19]. Inhibiting proliferation and inducing apoptosis in tumor cells are effective strategies to prevent tumor growth and eliminate cancers [20]. Although plenty of active ingredients of traditional Chinese medicine exhibit antitumor activities [21–23], their applications as antitumor agents are largely limited by the unknown mechanisms of action [24]. Previous studies have shown that SAN could induce apoptosis and inhibit the proliferation and
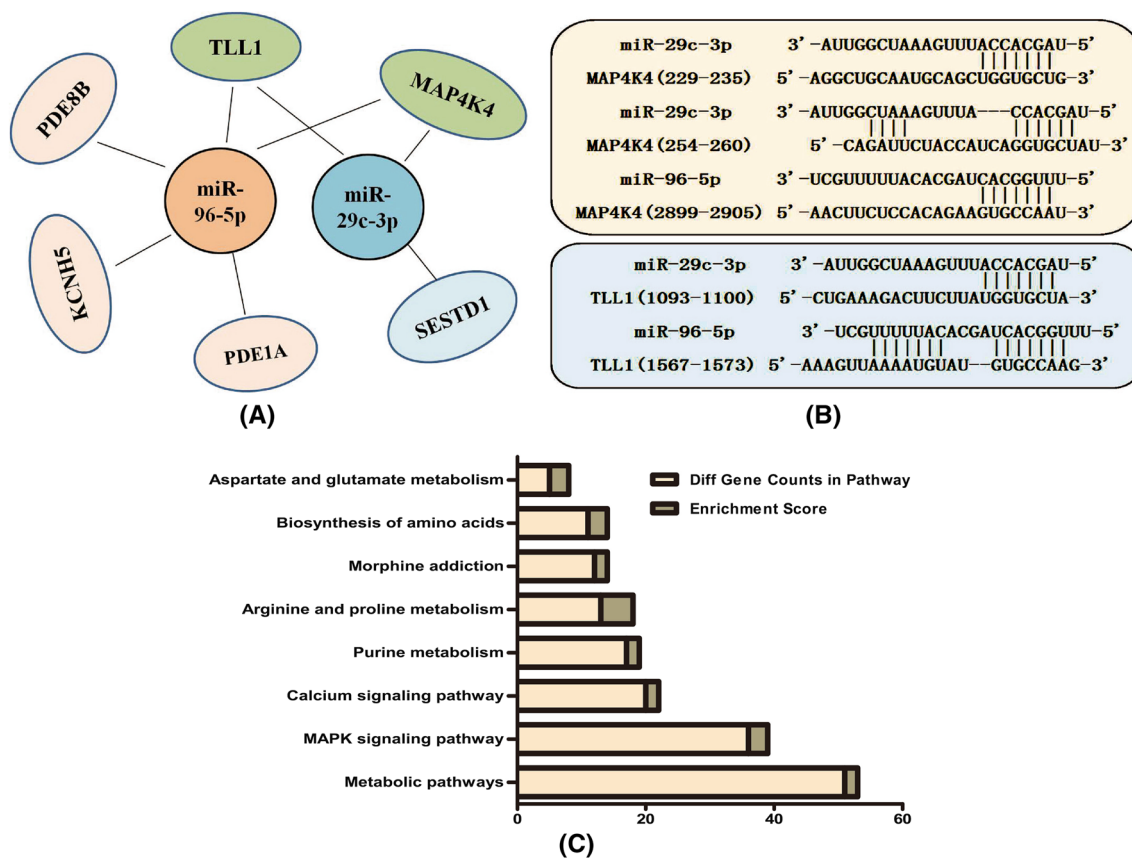
Fig. 6 Bioinformatic analysis of miR-29c-3p and miR-96-5p. (**a**) Possible target genes of miR-29c-3p and miR-96-5p. (**b**) Potential targeting (binding) sites of miR-96-5p and miR-29c-3p on MAP4K4 and TLL1 mRNAs predicted by TargetScan and miRanda software. (**c**) Possible enriched KEGG pathways of miR-29c-3p and miR-96-5p and their target genes

migration of tumor cells in multiple cancers, and is harmless to normal cells [16, 25–27]. However, so far the exact mechanism of the antitumor action of SAN has not yet been elucidated. Therefore, the present study aimed to determine the effect of SAN on the proliferation of GC cells and to elucidate the possible mechanism of its action, in hopes of proving experimental evidence for the clinical application of SAN in the treatment of GC.

The inhibitory effect of SAN on the viability of human GC cells in vitro was confirmed by CCK-8 assay. MGC-803 is originated from poorly differentiated human gastric mucinous adenocarcinoma, BGC-823 is originated from poorly differentiated human gastric adenocarcinoma, and SGC-7901 is originated from moderately differentiated human gastric adenocarcinoma with lymph node metastasis. SAN elicited concentration-dependent inhibition of the proliferation in MGC-803, BGC-823 and SGC-7901 cells, which was consistent with the proliferation inhibition effects of SAN in other cancers [28]. We chose the BGC-823 cell line to establish a subcutaneous xenograft tumor model in nude mice to evaluate the in vivo antitumor effect of SAN. Because the bioavailability of SAN was low via oral delivery

[29, 30], we administered SAN to the mice by intraperitoneal injection in the xenograft tumor model. We found that SAN also exhibited tumor growth inhibition effect in BGC-823 xenograft tumors in a dose-dependent manner. We further explored the molecular mechanism underlying the tumor growth inhibitory effect of SAN by gene microarray assay and identified eight differentially expressed miRNAs, including miR-194-3p, miR-148b-3p, miR-96-5p, miR-330-5p, miR-s454-3p, miR-29c-3p, miR-18b-5p, and miR-26b-5p. RT-PCR results showed that the expression of miR-96-5p, miR-29c-3p and their target gene MAP4K4 were consistent with gene microarray analysis results. Bioinformatics analysis of these differentially expressed genes showed that the pathways of these miRNAs and their target genes, such as MAPK signaling pathway and calcium signaling pathway, were closely related to cancer. KEGG pathway enrichment analysis revealed that MAP4K4 participates in the MAPK/JNK (c-Jun N-terminal kinase) signaling pathway. Subsequently, we found that SAN increased the expression of MAP4K4, pMEK4, and p-JNK1 proteins in tumors, suggesting that SAN may activate the MAPK/JNK pathway in these tumors.
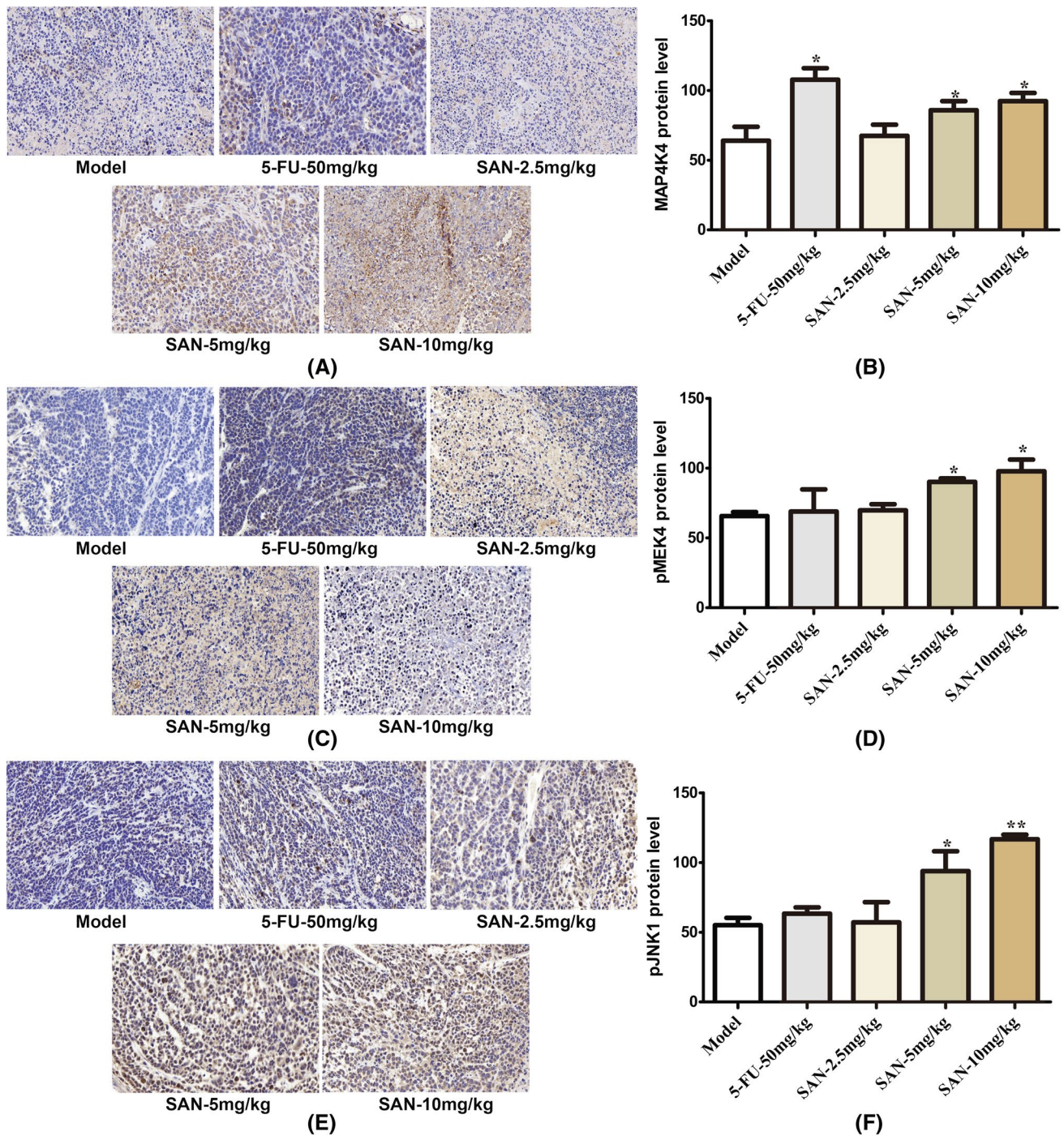
Fig. 7 Protein levels of MAP4K4, pMEK4 and pJNK1 in SAN treated BGC-823 xenograft gastric tumor tissues. The protein levels of MAP4K4, P-MEK4, and P-JNK1 in BGC-823 gastric tumor tissues following SAN treatment were determined by immunohisto-chemical staining using antibodies against MAP4K4, P-MEK4, and P-JNK1. Original magnification: ×400. *$P < 0.05$, **$P < 0.01$, compared with the model group

As a member of the serine threonine kinase family, MAPK is an important player of the major cell proliferation signaling pathway [31]. Activation of MAPK is associated with cell cycle arrest and apoptosis induction [32]. MAPK contains three major subfamilies: the extracellular-signal-regulated kinases (ERK), the JNK, and MAPK14 [33]. JNK is activated by environmental and genotoxic stresses and plays a key role in inflammation, cell proliferation, differentiation, survival, and migration of various cancer cells [34, 35]. The JNK pathway is crucial for the

activation of the mitochondria-mediated apoptotic pathway, which triggers the translocation of apoptotic protein Bax to mitochondria and the induction of apoptosis [36, 37]. Our study suggested that increased expression of MAP4K4 may promote the phosphorylation of MEKK1, which activates the downstream proapoptotic protein MKK4 through a cascade reaction, and subsequently activates the JNK pathway, resulting in proliferation inhibition. Previous studies have demonstrated that curcumin could activate JNK in cancer cells and induce a cascade reaction, leading to the BGC-823 cell apoptosis [38, 39]. Cyclin-dependent kinase 5 regulatory subunit associated protein 1 (CDK5RAP1) deficiency could cause cell cycle arrest and apoptosis in MCF-7 human breast cancer cells via the generation of ROS, thus activating JNK to induce apoptosis [40]. The role of JNK pathway in cancers is highly controversial. Studies have shown that the JNK signaling pathway is a dual functional one. It exerts both anti-tumor and pro-tumor activities, and the conversion depends on Ras [41]. The detailed mechanism of the anticancer action of SAN in gastric cancer remains to be further studied.

Conclusions

The present work demonstrated that SAN induced proliferation inhibition in BGC-823 gastric cancer cells through inhibiting miR-96-5p and miR-29c-3p expression and activating MAPK/JNK signaling pathway. Our finding provides a new insight into the molecular mechanism of SAN for cancer intervention and a reference for the discovery of novel diagnostic and therapeutic markers in gastric cancer.

Compliance with ethical standards

Conflict of interest The authors declare that there is no conflict of interest regarding the publication of this paper.

References

1. Ferro A, Peleteiro B, Malvezzi M, Bosetti C, Bertuccio P, Levi F, Negri E, La Vecchia C, Lunet N (2014) Worldwide trends in gastric cancer mortality (1980–2011), with predictions to 2015, and incidence by subtype. Eur J Cancer 50:1330–1344
2. Sasako M, Inoue M, Lin JT, Khor C, Yang HK, Ohtsu A (2010) Gastric cancer working group report. Jpn J Clin Oncol 40:i28–i37
3. Liu GH, Liu YH, Yang Z, Zhu AL, Zhao CL (2016) MicroRNA-524-5p suppresses the growth and invasive abilities of gastric cancer cells. Oncol Lett 11:1926–1932
4. Ferlay J, Shin HR, Bray F, Forman D, Mathers C, Parkin DM (2010) Estimates of worldwide burden of cancer in 2008: GLOBOCAN 2008. Int J Cancer 127:2893–2917
5. Zhang R, Wang G, Zhang PF, Zhang J, Huang YX, Lu YM, Da W, Sun Q, Zhu JS (2017) Sanguinarine inhibits growth and invasion of gastric cancer cells via regulation of the DUSP4/ERK pathway. J Cell Mol Med 21:1117–1127
6. Ajani JA, Bentrem DJ, Besh S, D'Amico TA, Das P, Denlinger C, Fakih MG, Fuchs CS, Gerdes H, Glasgow RE, Hayman JA, Hofstetter WL, Ilson DH, Keswani RN, Kleinberg LR, Korn WM, Lockhart AC, Meredith K, Mulcahy MF, Orringer MB, Posey JA, Sasson AR, Scott WJ, Strong VE, Varghese TK Jr, Warren G, Washington MK, Willett C, Wright CD, McMillian NR, Sundar H (2013) Gastric cancer, version 2.2013: featured updates to the NCCN guidelines. J Natl Compr Cancer Netw 11:531–546
7. Beuria TK, Santra MK, Panda D (2005) Sanguinarine blocks cytokines is in bacteria by inhibiting FtsZ assembly and bundling. Biochemistry 44:16584–16593
8. Adhami VM, Aziz MH, Mukhtar H, Ahmad N (2003) Activation of prodeath Bcl-2 family proteins and mitochondrial apoptosis pathway by sanguinarine in immortalized human HaCaT keratinocytes. Clin Cancer Res 9:3176–3182
9. Gu S, Yang XC, Xiang XY, Wu Y, Zhang Y, Yan XY, Xue YN, Sun LK, Shao GG (2015) Sanguinarine-induced apoptosis in lung adenocarcinoma cells is dependent on reactive oxygen species production and endoplasmic reticulum stress. Oncol Rep 34:913–919
10. Han MH, Park C, Jin CY, Kim GY, Chang YC, Moon SK, Kim WJ, Choi YH (2013) Apoptosis induction of human bladder cancer cells by sanguinarine through reactive oxygen species-mediated up-regulation of early growth response gene-1. PLoS One 8:e63425
11. Sun M, C Liu, Nadiminty N, Lou W, Zhu Y, Yang J, Evans CP, Zhou Q, Gao AC (2012) Inhibition of Stat3 activation by sanguinarine suppresses prostate cancer cell growth and invasion. Prostate 72:82–89
12. De Stefano I, Raspaglio G, Zannoni GF, Travaglia D, Prisco MG, Mosca M, Ferlini C, Scambia G, Gallo D (2009) Antiproliferative and antiangiogenic effects of the benzophenanthridine alkaloid sanguinarine in melanoma. Biochem Pharmacol 78:1374–1381
13. Singh CK, Kaur S, George J, Nihal M, Pellitteri Hahn MC, Scarlett CO, Ahmad N (2015) Molecular signatures of sanguinarine in human pancreatic cancer cells: a large scale label-free comparative proteomics approach. Oncotarget 6:10335–10348
14. Ahmad N, Gupta S, Husain MM, Heiskanen KM, Mukhtar H (2000) Differential antiproliferative and apoptotic response of sanguinarine for cancer cells versus normal cells. Clin Cancer Res 6:1524–1528
15. Kaminskyy V, Lin KW, Filyak Y, Stoika R (2008) Differential effect of sanguinarine, chelerythrine and chelidonine on DNA damage and cell viability in primary mouse spleen cells and mouseleukemic cells. Cell Biol Int 32:271–277
16. Zhang R, Wang G, Zhang PF, Zhang J, Huang YX, Lu YM, Da W, Sun Q, Zhu JS (2017) Sanguinarine inhibits growth and invasion of gastric cancer cells via regulation of the DUSP4/ERK pathway. J Cell Mol Med 21:1117–1127
17. Dong XZ, Zhang M, Wang K, Liu P, Guo DH, Zheng XL, Ge XY (2013) Sanguinarine inhibits vascular endothelial growth factor release by generation of reactive oxygen species in MCF-7 human mammary adenocarcinoma cells. Biomed Res Int 2013:517698
18. Xiao XY, Hao M, Yang XY, Ba Q, Li M, Ni SJ, Wang LS, Du X (2011) Licochalcone A inhibits growth of gastric cancer cells by arresting cell cycle progression and inducing apoptosis. Cancer Lett 302:69–75
19. Liang T, Zhang XJ, Xue WH, Zhao S, Zhang X, Pei J (2014) Curcumin induced human gastric cancer BGC-823 cells apoptosis by ROS-mediated ASK1-MKK4-JNK stress signaling pathway. Int J Mol Sci 15:15754–15765

20. Liu HM, Wu Q, Cao JQ, Wang X, Song Y, Mei WJ, Wang XC (2018) A phenanthroline derivative enhances radiosensitivity of hepatocellular carcinoma cells by inducing mitochondria-dependent apoptosis. Eur J Pharmacol 843:285–291

21. Lin X, Wei JB, Chen YX, He P, Lin J, Tan S, Nie J, Lu S, He M, Lu Z, Huang Q (2016) Isoorientin from Gypsophila elegans induces apoptosis in liver cancer cells via mitochondrial-mediated pathway. J Ethnopharmacol 187:187–194

22. Wu Y, Wang Y, Zhang Y, Chen LP, Wang JY (2014) Effect of matrine on NO and ADMA metabolism pathways in serum and tissues of mice with lipopolysaccharide-induced intestine tissue inflammation. China J Chin Mater Med 39:2318–2321

23. Jin H, Qiao F, Wang Y, Xu Y, Shang Y (2015) Curcumin inhibits cell proliferation and induces apoptosis of human non-small cell lung cancer cells through the upregulation of miR-192-5p and suppression of PI3K/Akt signaling pathway. Oncol Rep 34:2782–2789

24. Yu N, Xiong Y, Wang C (2017) Bu-Zhong-Yi-Qi decoction, the water extract of chinese traditional herbal medicine, enhances cisplatin cytotoxicity in A549/DDP cells through induction of apoptosis and autophagy. Biomed Res Int 2017:3692797

25. Zhang R, Wang G, Zhang PF, Zhang J, Huang YX, Lu YM, Da W, Sun Q, Zhu JS (2017) Sanguinarine inhibits growth and invasion of gastric cancer cells via regulation of the DUSP4/ERK pathway. J Cell Mol Med 21:1117–1127

26. Xu JY, Meng QH, Yu C, Jiao Y, Zhao L, Rosen EM, Fan S (2013) Sanguinarine is a novel VEGF inhibitor involved in the suppression of angiogenesis and cell migration. Mol Clin Oncol 1:331–336

27. Han MH, Kim GY, Yoo YH, Choi YH (2013) Sanguinarine induces apoptosis in human colorectal cancer HCT-116 cells through ROS-mediated Egr-1 activation and mitochondrial dysfunction. Toxicol Lett 220:157–166

28. De Stefano I, Raspaglio G, Zannoni GF, Travaglia D, Prisco MG, Mosca M, Ferlini C, Scambia G, Gallo D (2009) Antiproliferative and antiangiogenic effects of the benzophenanthridine alkaloid sanguinarine in melanoma. Biochem Pharmacol 78:1374–1381

29. Vecera R, Klejdus B, Kosina P, Orolin J, Stiborová M, Smrcek S, Vicar J, Dvorák Z, Ulrichová J, Kubán V, Anzenbacher P, Simánek V (2007) Disposition of sanguinarine in the rat. Xenobiotica 37(5):549–558

30. Satpathi S, Gavvala K, Hazra P (2015) Fluorescence switching of sanguinarine in micellar environments. Phys Chem Chem Phys 17(32):20725–20732

31. Kang HM, Park BS, Kang HK, Park HR, Yu SB, Kim IR (2018) Delphinidin induces apoptosis and inhibits epithelial-to-mesenchymal transition via the ERK/p38 MAPK-signaling pathway in human osteosarcoma cell lines. Environ Toxicol 33:640–649

32. Davis RJ (2000) Signal transduction by the JNK group of MAP kinases. Cell 103:239–252

33. Lee JT Jr, McCubrey JA (2002) The Raf/MEK/ERK signal transduction cascade as a target for chemotherapeutic intervention in leukemia. Leukemia 16:486–507

34. Karin M, Gallagher E (2005) From JNK to pay dirt: jun kinases, their biochemistry, physiology and clinical importance. IUBMB Life 57:283–295

35. Bubici C, Papa S (2014) JNK signalling in cancer: in need of new, smarter therapeutic targets. Br J Pharmacol 171:24–37

36. Lu YM, Zhu MY, Chen W, Yin L, Zhu J, Chen N, Chen W (2014) Oleanolic acid induces apoptosis of MKN28 cells via AKT and JNK signaling pathways. Pharm Biol 52:789–795

37. Fang JY, Richardson BC (2005) The MAPK signalling pathways and colorectal cancer. Lancet Oncol 6:322–327

38. Han X, Xu B, Beevers CS, Odaka Y, Chen L, Liu L, Luo Y, Zhou H, Chen W, Shen T, Huang S (2012) Curcumin inhibits protein phosphatases 2A and 5, leading to activation of mitogen-activated protein kinases and death in tumor cells. Carcinogenesis 33:868–875

39. Liang T, Zhang XJ, Xue WH, Zhao S, Zhang X, Pei J (2014) Curcumin induced human gastric cancer BGC-823 cells apoptosis by ROS-mediated ASK1-MKK4-JNK stress signaling pathway. Int J Mol Sci 15:15754–15765

40. Wang HB, Wei L, Li CL, Zhou J, Li Z (2015) CDK5RAP1 deficiency induces cell cycle arrest and apoptosis in human breast cancer cell line by the ROS/JNK signaling pathway. Oncol Rep 33:1089–1096

41. Enomoto M, Kizawa D, Ohsawa S, Igaki T (2015) JNK signaling is converted from anti- to pro-tumor pathway by Ras-mediated switch of Warts activity. Dev Biol 403:162–171

Publisher's Note Springer Nature remains neutral with regard to jurisdictional claims in published maps and institutional affiliations.